RAA 2014 Vol. **14** No. **10**, 1279–1288 doi: 10.1088/1674–4527/14/10/007
http://www.raa-journal.org *http://www.iop.org/journals/raa*

Research in Astronomy and Astrophysics

High spatial resolution spectroscopy of G292.0+1.8 with *Chandra* *

Xue-Juan Yang[1], Xiao-Qin Liu[1], Shun-Yu Li[1] and Fang-Jun Lu[2]

[1] Faculty of Materials, Optoelectronics and Physics, Xiangtan University, Xiangtan 411105, China; *xjyang@xtu.edu.cn*
[2] Particle Astrophysics Center, Institute of High Energy Physics, Chinese Academy of Sciences, Beijing 100049, China

Received 2014 March 1; accepted 2014 April 20

Abstract We present high spatial resolution X-ray spectroscopy of supernova remnant G292.0+1.8 made with *Chandra* observations. The X-ray emitting region of this remnant was divided into 25×25 pixels with a scale of $20'' \times 20''$ each. Spectra of 328 pixels were created and fitted with an absorbed one component non-equilibrium ionization model. With the spectral analysis results, we obtained maps of absorbing column density, temperature, ionization age and abundances for O, Ne, Mg, Si, S and Fe. The abundances of O, Ne and Mg show tight correlations between each other in the range of about two orders of magnitude, suggesting that they are all from explosive C/Ne burning. Meanwhile, the abundances of Si and S are also well correlated, indicating that they are the ashes of explosive O-burning or incomplete Si-burning. The Fe emission lines are not prominent in the whole remnant, and their abundance is significantly reduced, indicating that the reverse shock may not have propagated to the Fe-rich ejecta. Based on relative abundances of O, Ne, Mg, Si and Fe to Si, we suggest a progenitor mass of $25 - 30\ M_{\odot}$ for this remnant.

Key words: ISM: supernova remnants — ISM: individual: G292.0+1.8

1 INTRODUCTION

G292.0+1.8, also known as MSH 11–54, is a bright Galactic supernova remnant (SNR). It is relatively young with an age of $\leq 1600\ \mathrm{yr}$ (Murdin & Clark 1979). The detection of strong O and Ne lines in the optical spectrum (Goss et al. 1979; Murdin & Clark 1979) classified G292.0+1.8 as one of the only three known O-rich SNRs in the Galaxy. The others are Cassiopeia A and Puppis A.

G292.0+1.8 was first detected in X-ray with *HEAO* 1. With the increasing sensitivity and resolution of subsequent X-ray satellites, finer structures have been revealed, such as the central bar-like feature (Tuohy et al. 1982), metal rich ejecta around the periphery and thin filaments with normal composition centered on and extending nearly continuously around the outer boundary (Park et al. 2002). The equivalent width (EW) maps of O, Ne, Mg and Si clearly show regions with enhanced metallicity for these elements (Park et al. 2002). G292.0+1.8 is bright in O, Ne, Mg and Si and weaker in S and Ar with little Fe, suggesting that the ejecta is strongly stratified by composition and that the reverse shock has not propagated to the Si/S- or Fe-rich zones (Park et al. 2004; Ghavamian

* Supported by the National Natural Science Foundation of China.

et al. 2012). Meanwhile, the central bar-like belt has a normal chemical composition, suggesting it originated from shocked dense circumstellar material (Park et al. 2004; Ghavamian et al. 2005).

The detection of the central pulsar (PSR J1124−5916) and its wind nebula (Hughes et al. 2001, 2003; Camilo et al. 2002; Gaensler & Wallace 2003; Park et al. 2007) demonstrates G292.0+1.8 comes from a core-collapse SNR. The progenitor mass has been investigated. Hughes & Singh (1994) suggested a progenitor mass of $\sim 25\,M_{\odot}$ by comparing the derived element abundances of O, Ne, Mg, Si, S and Ar with those predicted by the numerical nucleosynthesis calculation based on *EXOSAT* data. Gonzalez & Safi-Harb (2003) estimated it to be $\sim 30-40\ M_{\odot}$ with the same method as used by *Chandra* observations.

In this paper, we present spatially resolved spectroscopy of G292.0+1.8, using *Chandra* ACIS observations. In previous work, several typical regions have been selected and their spectra were analyzed (e.g. Gonzalez & Safi-Harb 2003, hearafter GS03; Vink et al. 2004; Lee et al. 2010) or the EW maps were given (Park et al. 2002). We, for the first time, systematically derive high spatially resolved spectroscopy for this SNR. In Sections 2 and 3, we present observational data and results respectively. In Section 4, we discuss nucleosynthesis and the progenitor mass. A summary is given in Section 5.

2 OBSERVATION AND DATA REDUCTION

G292.0+1.8 was observed by the ACIS-S3 chip on board *Chandra* on 2000–03–11 from 00:05:46 to 13:21:46 UTC with observation ID 126. After screening the data, the net exposure time was about 43 ks.

The X-ray data were analyzed using the software package CIAO (version 4.1). In this paper, we divided the X-ray emission region into 25 × 25 grids with "pixel" size of $20'' \times 20''$. We extracted events within energy range 0.5−10 keV and created spectra for 328 pixels.

Figure 1 shows the image of this observation with the grid overlaid. The background spectrum was created from the off-source region.

The spectra were fitted within XSPEC software package (version 11.3, Arnaud 1996), using one non-equilibrium ionization component (VNEI, Borkowski et al. 2001). The free parameters are the temperature, emission measure, ionization age ($\tau = n_{\rm e}t$) and abundances of O, Ne, Mg, Si, S and Fe (in units of solar abundances given by Anders & Grevesse 1989). The reason these elements' abundances are free parameters is that they show prominent emission lines in the spectra (cf. Fig. 3). We also introduced the WABS model (Morrison & McCammon 1983) for interstellar photoelectric absorption.

3 RESULTS

Figure 2 shows the frequency distribution of the 328 reduced χ^2 values computed from spectral fits, which peaks around 0.85, suggesting the fitting results are statistically acceptable.

In Figure 3, we give the spectra along with the fitting residuals of several typical regions (marked in Fig. 1). Region A is the O/Ne-rich region, with strong O and Ne lines and very weak Si and S lines. The abundances for O, Ne and Mg are above 4.0 but $\leq$0.3 for Si and S. As an O-rich SNR, such a region is very typical. Region B, on the other hand, shows strong Si and S lines, and relatively weak O and Ne lines. It has a much higher abundance for Si and S ($\sim$ 2.0), but much lower abundance for O, Ne and Mg ($\sim$ 3.0) than region A. Region C is from the central bright belt area, which shows very strong continuum and emission lines from medium-mass elements, such as Si, S and Ca. The abundance for all the metal elements is significantly reduced ($0.3-0.5$). Region D covers the central pulsar. A very strong hard continuum tail is observed from the spectrum. O, Ne and Mg lines are clearly shown but no emission lines are seen above 1.8 keV. Fe-K lines, however, are not detected in any of these regions.

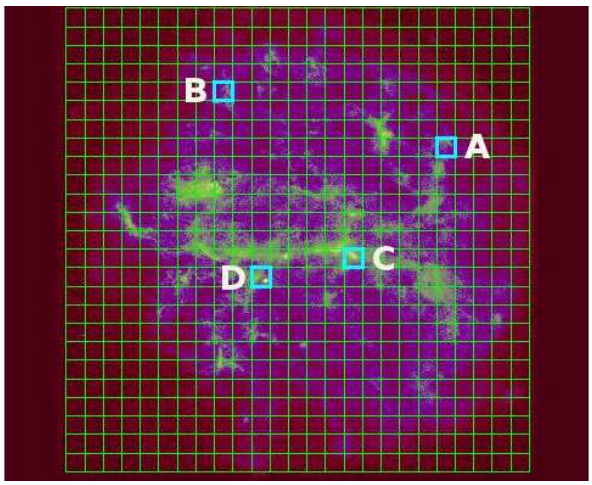

Fig. 1 The pixel grid used in our analyses superimposed on the *Chandra* image of G292.0+1.8.

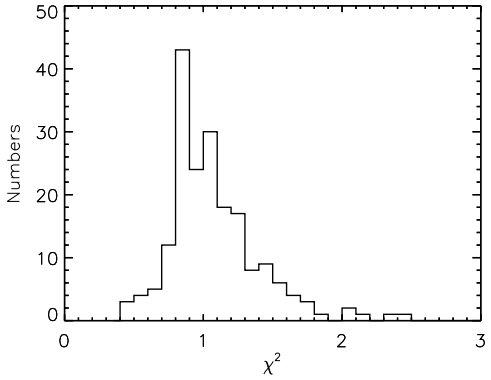

Fig. 2 Frequency distribution of the 328 χ^2 values computed from the spectral fits.

The emission lines from O have been detected in the O-rich region (A), the Si-rich region (B) and even the region dominated by the pulsar (D). However, the central bar-like feature (shown by region C), although it is very bright, shows very weak O emission. This supports the theory that such a belt should originate from the shocked circumstellar medium, rather than metal-rich ejecta (Park et al. 2002). The hard tail in the spectrum of region D is due to the pulsar. The photon index is 1.87 ± 0.09, which is consistent with the value given by GS03 (1.74 ± 0.10) and Hughes et al. (2003; 1.6) and the typical photon index of a pulsar ($1.5-2.0$, Becker 2009).

(I) The spatial distributions of the fitted parameters.

The spatial distributions of the absorbing column density, temperature and the ionization ages are shown in Figure 4. The column density for this SNR lies in the range $0.2-0.7\times10^{22}$ cm^{-2}, with a mean value $\sim\ 0.45\times10^{22}$ cm^{-2}. This is consistent with previous results (Park et al. 2004). The column density map is relatively uniform, suggesting there are no extra absorbing materials around

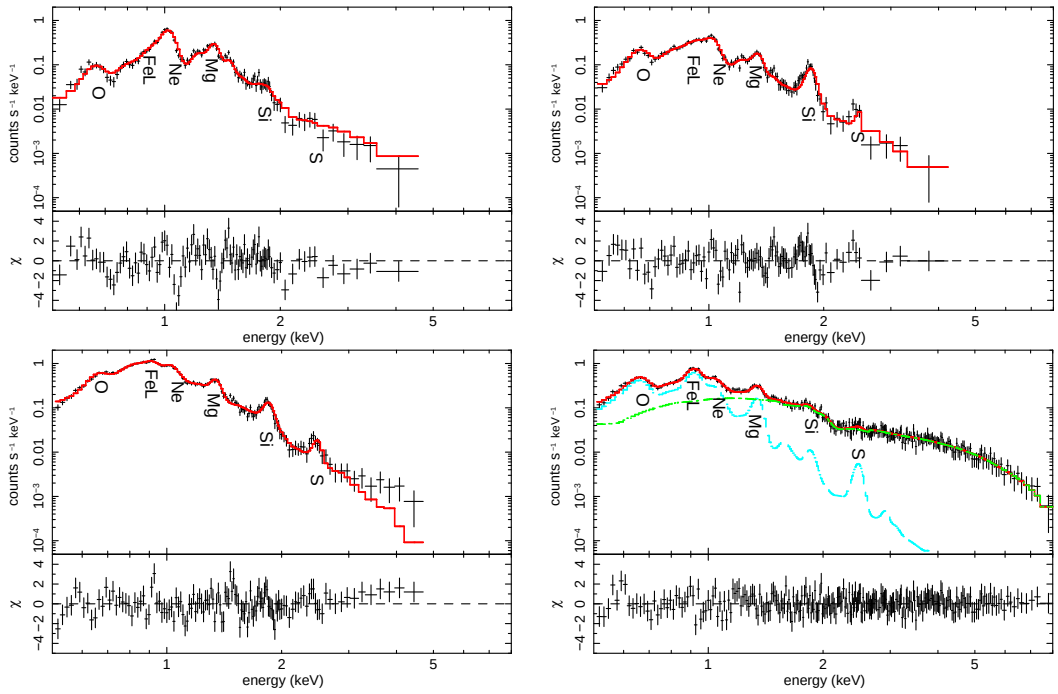

Fig. 3 Spectra along with the fitting results for typical regions as denoted in Fig. 1. Region A: top left; Region B: top right; Region C: bottom left; Region D: bottom right.

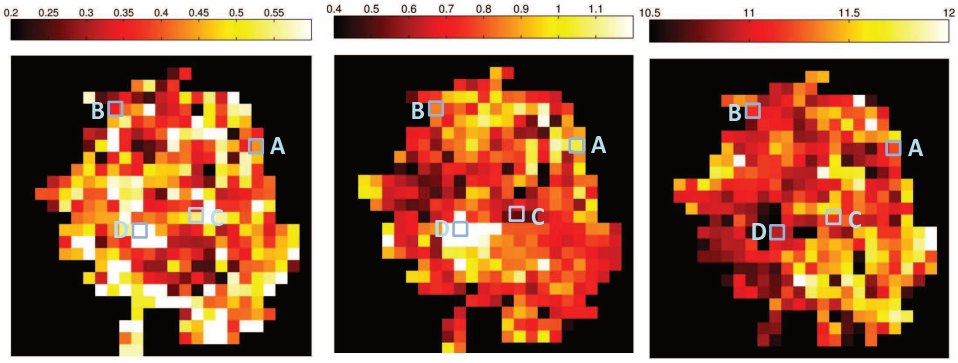

Fig. 4 Maps showing the absorbing column density ($N_{\rm H}$, 10^{22} cm^{-2}, *left panel*), temperature (kT, keV, *middle panel*) and ionization age ($\log_{10} n_{\rm e}t$ cm^{-3} s, *right panel*) of G292.0+1.8. The coding used is shown on the top of each panel. Regions A/B/C/D as shown in Fig. 1 are marked here.

this SNR. The temperatures are typically $0.5-1.0$ keV. The relatively "hot" regions are those around the pulsar wind nebula; the "high" temperatures are perhaps not real but rather contamination from the non-thermal emission of the pulsar wind nebula. The central bright belt of G292.0+1.8 was attributed to the forward shocked circumstellar medium (Park et al. 2002), which should have a larger electron density ($n_{\rm e}$) and longer time when the shock influences it (t). Its ionization age,

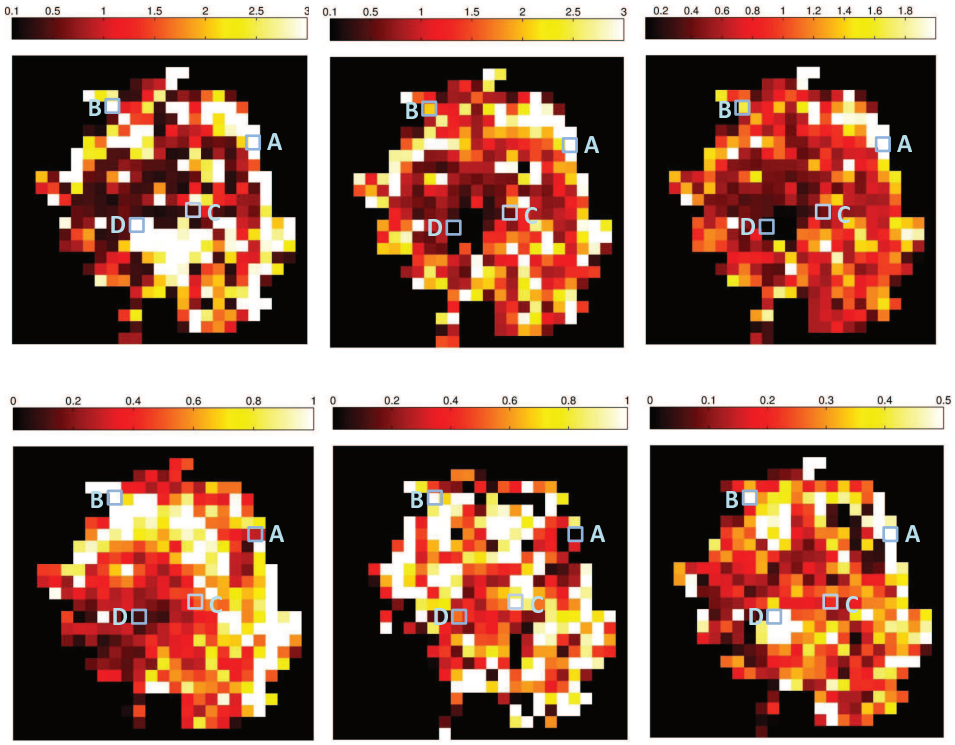

Fig. 5 Maps of O (*top left*), Ne (*top middle*), Mg (*top right*), Si (*bottom left*), S (*bottom middle*) and Fe (*bottom right*) abundance (in units of solar abundance) for G292.0+1.8. Regions A/B/C/D as shown in Fig. 1 are marked here.

$\log_{10}(n_{\rm e}t)$, however, is even smaller than that in the other regions. The reason might be that these materials have reached ionization equilibrium, and the ionization age we give here is obtained from a non-equilibrium model and thus not reliable for these regions.

The spatial distributions of all the fitted elements are shown in Figure 5. It is clear that the central bar-like structure is not enhanced in any of these elements. This supports it originating from circumstellar materials (Park et al. 2004; Ghavamian et al. 2005). In the meantime, no clear stratification of the element abundances is observed from these maps. The distributions of the Ne and Si enhanced regions are generally consistent with their EW maps obtained by Park et al. (2002).

(II) Correlations shown by element abundances.

Figure 6 shows the correlation plots of the abundances of O and Ne with other elements, and Figure 7 shows the correlation of Si and Fe with the others. The points with minimum element abundances ($\sim$20% of the total data points, i.e. the very dark regions in each of the panels of Fig. 5) are excluded, since they represent regions with very weak metal emission lines and thus are probably dominated by the continuum. The coherent coefficients (ρ) are given in Table 1, along with the corresponding values obtained in Cas A (Yang et al. 2008).

The first conclusion that can be drawn from Table 1 and Figures 6 and 7 is that in G292.0+1.8 the abundances of O, Ne and Mg show a good correlation with each other, as do those for Si vs. S. Such a correlation pattern can also be found in Cas A (cf. Table 1), although the coherent coefficients

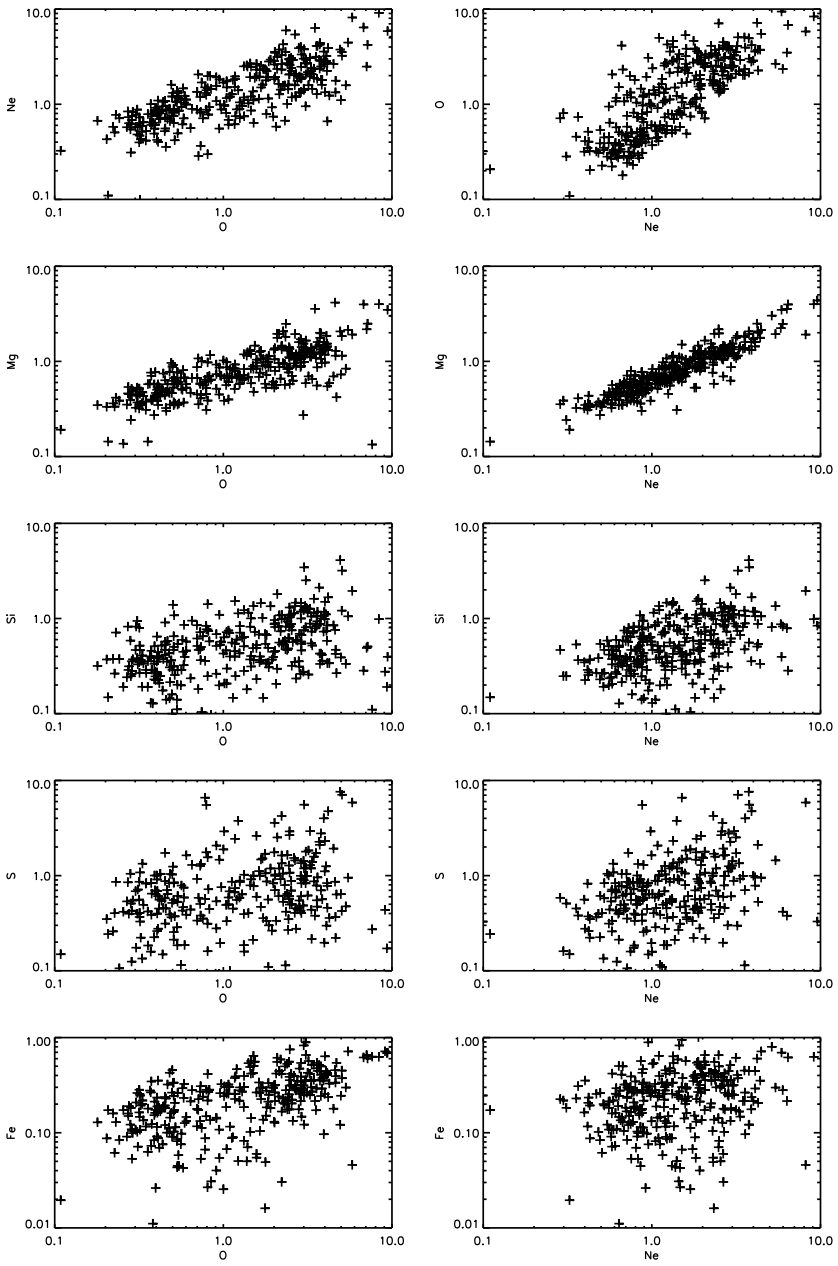

Fig. 6 Abundance correlations between O/Ne and the other elements.

are different. For example, the most correlated pair in G292.0+1.8 is Ne and Mg, with $\rho = 0.88$, but in Cas A this coefficient is 0.49. The second conclusion is that the Fe abundance is basically not correlated with that of any other element. However, the two phase correlation between Si and Fe abundance found in Cas A (fig. 8 in Yang et al. 2008) was not shown in G292.0+1.8. These will be discussed in Section 4.1.

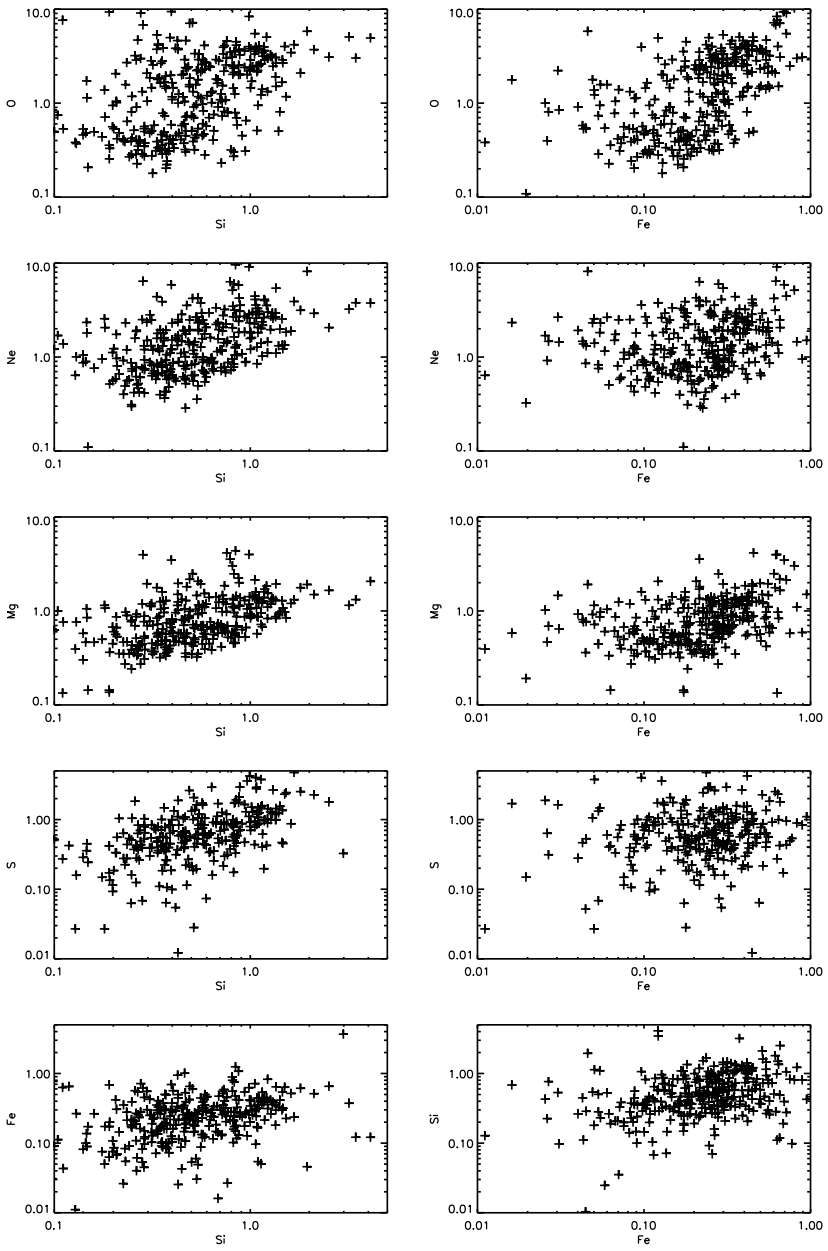

Fig. 7 Abundance correlations between Si/Fe and the other elements.

4 DISCUSSION

4.1 Nucleosynthesis

The O, Ne and Mg abundances show tight correlations with each other within the range of about two orders of magnitude. This is strong evidence that they all come from the explosive C/Ne burning.

Table 1 Coherent coefficient for data points excluding extremum cases. The corresponding values for Cas A (Yang et al. 2008) are given in parentheses.

Element	O	Ne	Mg	Si	S	Fe
O	–	0.64(0.33)	0.66(0.41)	0.58(0.33)	0.45(0.26)	0.43(0.13)
Ne	0.64(0.33)	–	0.88(0.49)	0.47(0.19)	0.41(0.16)	0.03(0.25)
Mg	0.66(0.41)	0.88(0.49)	–	0.52(0.48)	0.29(0.39)	0.24(0.24)
Si	0.58(0.33)	0.47(0.19)	0.52(0.48)	–	0.70(0.86)	0.31(0.23)
S	0.45(0.26)	0.41(0.16)	0.29(0.39)	0.70(0.86)	–	0.01(0.11)
Fe	0.43(0.13)	0.03(0.25)	0.24(0.24)	0.31(0.23)	0.01(0.11)	–

Moreover, such correlation is also found between Si and S abundance, suggesting they are ashes of explosive O-burning and incomplete Si-burning in the core-collapse supernova. This kind of correlation pattern for elemental abundance is very similar to Cas A (Yang et al. 2008), and is also consistent with the (explosive) nucleosynthesis calculations for a massive star (Woosley et al. 2002; Woosley & Janka 2005). The difference between G292.0+1.8 and Cas A is that the former SNR is O-rich while the latter one is Si-rich.

In Cas A, the Fe abundance is positively correlated with that of Si when Si abundance is lower than three solar abundances, and a negative correlation appears when the Si abundance is higher (Yang et al. 2008). It is suggested that the Si-rich regions are the ejecta of incomplete explosive Si-burning mixing with O-burning products, and the regions with lower Si abundance might be dominated by the shocked circumstellar medium (CSM). In G292.0+1.8, we can only find a weak positive correlation between Si and Fe abundance in the whole remnant. This is not surprising because no prominent Fe lines have been detected in most of the regions in G292.0+1.8, and thus the Fe abundance cannot be that well-constrained. In addition, both Si and Fe are not enriched in the SNR, with their abundances smaller than one solar abundance. This, again, confirms that the reverse shock may not have propagated into the Fe-rich ejecta (Park et al. 2004; Ghavamian et al. 2009, 2012).

4.2 Progenitor Mass

Theoretical calculations have suggested that for core-collapse supernovae, a different progenitor mass will yield a very different abundance pattern (Woosley & Weaver 1995, etc). Gonzalez & Safi-Harb (2003) suggested that the progenitor mass of G292.0+1.8 could be around $30-40\ M_{\odot}$ based on a comparison of the observed abundance ratios with theoretical values. Their abundance ratios are taken from several ejecta-dominated regions within this SNR.

Here we gave the emission-measure-weighted average abundance for O, Ne, Mg, Si, S and Fe in the whole remnant and their root mean square (rms) (Z and σ_Z in Table 2). To compare with GS03's work, we also give the abundance ratio of all the elements with respect to Si and their rms ($Z/Z_{\rm Si}$ and $\sigma_{Z/Z_{\rm Si}}$ in Table 2). By taking G03's observational value and theoretical values they employed, we overplotted our measurements in Figure 8. The abundance ratios measured here are systematically lower than those from GS03. One might wonder that the reason could be that the shocked CSM regions are included in our calculation. Considering this, we artificially choose the ejecta-dominated region by the standard of the O abundance larger than 1.0, and calculated the corresponding ratio again (Table 2, $(Z/Z_{\rm Si})'$). We can see that values for $(Z/Z_{\rm Si})'$ are generally consistent with $Z/Z_{\rm Si}$ within the scatter. This is not surprising for two reasons. One is that the Si abundance is tentatively correlated with other elements. The other is that the larger values of element abundance contribute much more to the final average values, so that even though the average abundance is much larger, their ratios tend to be similar. Our measurements suggest the progenitor mass for G292.0+1.8 is $25-30\ M_{\odot}$, smaller than $30-40\ M_{\odot}$ suggested by GS03.

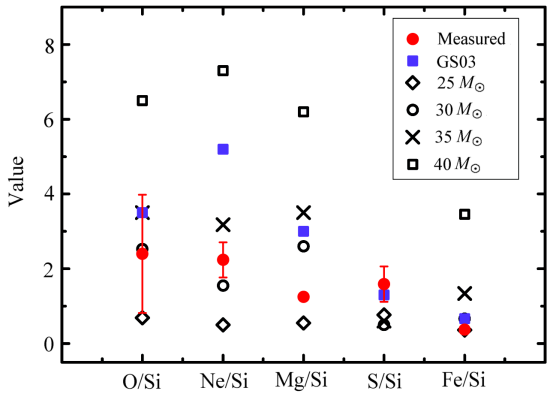

Fig. 8 Average abundance ratio and their rms scatter, compared with Gonzalez & Safi-Harb (2003) and theoretical values.

Table 2 Average abundance weighted by emission measure and their ratios with respect to Si.

Element	O	Ne	Mg	Si	S	Fe
Z	1.32	1.24	0.69	0.55	0.88	0.20
σ_Z	1.03	0.41	0.09	0.07	0.38	0.01
$Z/Z_{\rm Si}$	2.40	2.24	1.25	–	1.59	0.37
$\sigma_{Z/Z_{\rm Si}}$	1.58	0.47	0.01	–	0.47	0.03
$(Z/Z_{\rm Si})'$	3.29	2.54	1.30	–	1.53	0.35

Z: Average abundance weighted by emission measure; σ_Z: Weighted standard deviation for Z; $Z/Z_{\rm Si}$: Elemental abundance ratio with respect to Si; $\sigma_{Z/Z_{\rm Si}}$: Standard deviation for $Z/Z_{\rm Si}$; $(Z/Z_{\rm Si})'$: Average abundance weighted by emission measure for the regions with O abundance greater than 1.0.

5 SUMMARY

We performed spatially resolved X-ray spectroscopy of SNR G292.0+1.8. The spatial distributions of the absorption column density, temperature, ionization age and abundances of O, Ne, Mg, Si, S and Fe are given. The uniform column density map suggests there is no extra absorbing material around this SNR. The central bright belt (with larger electron density and a longer time when the shock influences it) shows smaller ionization age than other regions. All of the element abundance maps show no clear stratification. The central bar-like structure is not enhanced in any of the element abundances, supporting it originating from shocked circumstellar material. The Fe emission lines are not prominent in the whole remnant, and its abundance is significantly reduced, indicating that the reverse shock may not have propagated to the Fe-rich ejecta. The O/Ne/Mg abundances show tight correlations with each other, as do those for Si/S. Such correlations suggest a common origin of nucleosynthesis for O/Ne/Mg and Si/S. Based on relative abundances of O, Ne, Mg, Si and Fe to Si, we suggest a progenitor mass of $25-30\ M_\odot$ for G292.0+1.8.

Acknowledgements We acknowledge the use of data obtained by *Chandra*. The Chandra Observatory Center is operated by the Smithsonian Astrophysical Observatory for and on behalf of NASA. This project is supported by the National Natural Science Foundation of China (Grant Nos. 10903007, 11273022 and 11473023).

References

Anders, E., & Grevesse, N. 1989, Geochim. Cosmochim. Acta, 53, 197
Arnaud, K. A. 1996, in Astronomical Society of the Pacific Conference Series, 101, Astronomical Data Analysis Software and Systems V, eds. G. H. Jacoby, & J. Barnes, 17
Becker, W. 2009, in Astrophysics and Space Science Library, 357, Astrophysics and Space Science Library, ed. W. Becker, 91
Borkowski, K. J., Lyerly, W. J., & Reynolds, S. P. 2001, ApJ, 548, 820
Camilo, F., Manchester, R. N., Gaensler, B. M., Lorimer, D. R., & Sarkissian, J. 2002, ApJ, 567, L71
Gaensler, B. M., & Wallace, B. J. 2003, ApJ, 594, 326
Ghavamian, P., Hughes, J. P., & Williams, T. B. 2005, ApJ, 635, 365
Ghavamian, P., Raymond, J. C., Blair, W. P., et al. 2009, ApJ, 696, 1307
Ghavamian, P., Long, K. S., Blair, W. P., et al. 2012, ApJ, 750, 39
Gonzalez, M., & Safi-Harb, S. 2003, ApJ, 583, L91
Goss, W. M., Shaver, P. A., Zealey, W. J., Murdin, P., & Clark, D. H. 1979, MNRAS, 188, 357
Hughes, J. P., & Singh, K. P. 1994, ApJ, 422, 126
Hughes, J. P., Slane, P. O., Burrows, D. N., et al. 2001, ApJ, 559, L153
Hughes, J. P., Slane, P. O., Park, S., Roming, P. W. A., & Burrows, D. N. 2003, ApJ, 591, L139
Lee, J.-J., Park, S., Hughes, J. P., et al. 2010, ApJ, 711, 861
Morrison, R., & McCammon, D. 1983, ApJ, 270, 119
Murdin, P., & Clark, D. H. 1979, MNRAS, 189, 501
Park, S., Roming, P. W. A., Hughes, J. P., et al. 2002, ApJ, 564, L39
Park, S., Hughes, J. P., Slane, P. O., et al. 2004, ApJ, 602, L33
Park, S., Hughes, J. P., Slane, P. O., et al. 2007, ApJ, 670, L121
Tuohy, I. R., Burton, W. M., & Clark, D. H. 1982, ApJ, 260, L65
Vink, J., Bleeker, J., Kaastra, J. S., & Rasmussen, A. 2004, Nuclear Physics B Proceedings Supplements, 132, 62
Woosley, S., & Janka, T. 2005, Nature Physics, 1, 147
Woosley, S. E., Heger, A., & Weaver, T. A. 2002, Reviews of Modern Physics, 74, 1015
Woosley, S. E., & Weaver, T. A. 1995, ApJS, 101, 181
Yang, X.-J., Lu, F.-J., & Chen, L. 2008, ChJAA (Chin. J. Astron. Astrophys.), 8, 439